



Towards locating time-varying indoor particle sources: Development of two multi-robot olfaction methods based on whale optimization algorithm

Yibin Yang^b, Boyuan Zhang^a, Qilin Feng^d, Hao Cai^{a,*}, Mingrui Jiang^a, Kang Zhou^a, Fei Li^a, Shichao Liu^e, Xianting Li^c



^a Department of HVAC, College of Urban Construction, Nanjing Tech University, Nanjing, 210009, PR China

^b College of National Defense Engineering, Army Engineering University, Nanjing, 210007, PR China

^c Department of Building Science, Tsinghua University, Beijing, 100084, PR China

^d Research Institute for National Defense Engineering of Academy of Military Science PLA China, Beijing, 100850, PR China

^e Department of Civil and Environmental Engineering, Worcester Polytechnic Institute, Worcester, MA, 01609, USA

ARTICLE INFO

Keywords:

Indoor particle pollution
Source localization
Time-varying source
Mobile robot olfaction
Whale optimization algorithm (WOA)
Particle swarm optimization (PSO)

ABSTRACT

Source localization is crucial for controlling indoor particle pollution. Locating indoor particle sources is challenging because the dispersion of particles is more complicated than that of gases, and the release rates of particle sources usually change with time in real-world applications. This study presents two multi-robot olfaction methods based on the newly emerging whale optimization algorithm (WOA), namely, the standard WOA (SWOA) and improved WOA (IWOA) methods, for locating time-varying indoor particle sources without and with airflow information, respectively. By combining experiments and CFD simulations, the presented methods were validated and compared with two particle swarm optimization (PSO)-based methods, namely, standard PSO (SPSO) and improved PSO (IPSO) methods. Four typical scenarios, including two time-varying source types (decaying source and periodic source) and two ventilation modes (displacement ventilation and mixing ventilation), were simulated and exported as virtual environments to test these methods. The methods were evaluated by the success rate (the number of successful experiments divided by the number of total experiments) and the average localization time of the experiments. The results showed that the SWOA method outperformed the SPSO method with a higher success rate (SWOA: 66.00%, SPSO: 52.00%) and a less average localization time (SWOA: 65.48 s, SPSO: 69.65 s) for all four scenarios. The IWOA method performed slightly better in success rate (IWOA: 97.75%, IPSO: 97.00%), while the IPSO method performed slightly better in average localization time (IWOA: 42.18 s, IPSO: 39.18 s) for all four scenarios. In addition, the most cost-effective anemometer was also determined.

1. Introduction

Indoor airborne particles are closely related to human health and safety. Studies have shown that indoor exposure of particles is related to cardiovascular and pulmonary damages [1,2], and this relationship becomes more evident for higher intensity and longer duration exposure [3]. In addition, some infectious viruses (SARS, H1N1-A, etc.) can also be transmitted through aerosol inhalation, leading to the outbreak of epidemics [4–6]. In some extreme cases, such as terrorist attacks that release chemical or biological aerosols [7,8], hazardous particles can even threaten human lives. Therefore, controlling indoor particle pollution and ensuring the health and safety of indoor people motivate the study of developing effective methods for locating indoor particle sources, which can play an important role in source control,

pollution isolation, ventilation and purification [9].

Existing source localization methods can be roughly divided into two categories: stationary sensor network methods and mobile robot olfaction methods. Stationary sensor network methods use “forward” [10,11] or “backward” [12–16] models to estimate the source location based on the contaminant concentrations detected by the sensor network. This type of method usually requires performing forward or backward numerical simulations of contaminant dispersion, such as computational fluid dynamics (CFD) simulations. In addition, this type of method requires the sensor network to be deployed in indoor environments in advance. Therefore, this type of method cannot be applied to emergency situations where the sensor network is not pre-deployed but source localization is required, and situations where the predeployed sensor network is damaged in the event of an earthquake

* Corresponding author.

E-mail address: caihao@njtech.edu.cn (H. Cai).

or explosion.

Mobile robot olfaction methods utilize single or multiple robots equipped with anemometers and contaminant sensors to search for and locate the contaminant source. This type of method normally divides the source localization process into three subtasks: plume finding, plume tracking, and source declaration [17]. Mobile robot olfaction methods usually mimic the uncanny behaviors of natural creatures to locate sources, such as mating by moths, foraging by lobsters, and prey tracking by blue crabs [18,19]. Therefore, this type of method normally does not rely on numerical simulations and can be easily applied to mobile robots available on the market. In addition, robots can be quickly deployed at emergency sites, which makes the mobile robot olfaction methods can be applied to unknown environments in some unexpected situations.

To date, most previous studies on source localization have focused on locating indoor gas sources with constant release rates [20–23], and only a few studies have considered indoor particle sources [15,24]. One reason may be that, particle source localization is associated with enhanced uncertainties than that of gas pollutants due to the uniqueness that is not necessarily shared with gases, such as coincidence loss, particle aggregation, and deposition loss [25,26]. Another reason may be that the release rates of particles usually vary with time (e.g., the pressurized bioaerosol from small spray device [27] and the respiratory activities of patients infected by SARS or H1N1-A [28]). The time-varying characteristics of the release rates of particles can add more uncertainties to the already complex source localization. Therefore, we focused on time-varying particle sources in this study to understand to what extent the presented methods can successfully and effectively locate indoor particle sources. It is expected that a robust method for locating time-varying particle sources performs better when considering gas sources, but not vice versa.

In recent years, multi-robot olfactory methods for source localization based on swarm intelligence theory have received increasing attention [18,19]. Typical methods include particle swarm optimization (PSO) [29–33], ant colony optimization (ACO) [22], and adapted methods [34,35]. Among these methods, PSO-based methods have attracted the attention of many researchers due to their rapid convergence, high-efficiency cooperation, and simple implementation features [24,30,36]. Nevertheless, the standard PSO method (SPSO) can easily become trapped in a local extremum area because of its poor exploration ability [36]. In our previous study, we presented an improved PSO method (IPSO) by adding an upwind term to the SPSO method [24]. This IPSO method can help robots successfully escape from local extremum areas by using airflow information. However, when robots adopt the IPSO method, they tend to come together prematurely, thus losing the opportunity to explore more space.

In 2016, Mirjalili et al. presented a biological-inspired optimization algorithm called the whale optimization algorithm (WOA) [37]. As a newly emerging algorithm, the WOA has demonstrated excellent exploration ability and outperformed the PSO algorithm while escaping from local optima [37]. Although the WOA has been widely used in many applications such as computer vision [38], scheduling problems [39], and optimal siting [40] in the last three years, to the best of our knowledge, this algorithm has not been applied to source localization. Inspired by the successful applications of the WOA in other fields, the purpose of this study is to adapt the WOA to solve the problem of source localization by using its superior exploration ability and determine whether WOA-based methods can outperform PSO-based methods in locating indoor time-varying particle sources.

To achieve the above purpose, we present two multi-robot olfaction methods based on the WOA, namely, standard WOA (SWOA) and improved WOA (IWOA) methods, for locating indoor time-varying particle sources without and with airflow information, respectively. The SWOA method uses only concentration information. Therefore, when using this method, the robots do not need to be equipped with anemometers, as those currently available on the market are generally expensive and

bulky. The SWOA method can help reduce the cost of source localization systems and is suitable for narrow or congested environments and for situations where anemometers cannot be carried, such as nano aerial vehicles (NAVs) [41]. The IWOA method uses both concentration and airflow information to improve the efficiency of source localization. This method is suitable for applications where the robots can be equipped with anemometers. In addition, to determine the most cost-effective anemometer for source localization, we also investigated the effects of anemometer measurement thresholds on the performance of source localization.

The presented SWOA and IWOA methods were validated by a combination of experiments and CFD simulations and were compared with the SPSO and IPSO methods, respectively. The feasibility of the CFD method was validated by comparing the results of CFD simulation with the measurements of airflow profiles and particle concentrations in an experimental chamber. Based on a model of the experimental chamber, four typical scenarios, which represent the combinations of two source types (decaying source and periodic source) and two ventilation modes (mixing ventilation and displacement ventilation), were simulated and exported as virtual environments to test and compare the WOA-based and PSO-based methods. In the comparison of the IWOA and IPSO methods, anemometers with measurement thresholds of 0.1 m/s, 0.05 m/s and 0.01 m/s were tested to determine the most cost-effective anemometer for source localization. To obtain statistically significant results, each method was tested 100 times in each case (supported by conducting statistical tests), and a total of 3200 experiments were conducted for evaluating the methods.

2. Development of two WOA-based multi-robot olfaction methods

2.1. Framework and procedure

Fig. 1 shows the framework and procedure of the two WOA-based methods. In each method, the source localization process is divided into the following three subtasks:

- (1) Plume finding: The robots use a random divergence strategy to find the plume. According to this strategy, each robot starts from a random position and moves in a random direction along a straight line. When any of the robots detects a concentration higher than the preset threshold of plume tracking C_t , the robots will end the plume finding subtask and switch to the plume tracking subtask.
- (2) Plume tracking: Two WOA-based algorithms, namely, SWOA and IWOA, were developed to track the plume. For the SWOA, the robots track the plume using only concentration information. For the IWOA, by adding an upwind term to the SWOA, the robots can move upwind while approaching the high-concentration area during the plume tracking subtask. These two algorithms are described in detail in Sections 2.2 and 2.3, respectively. During the plume tracking subtask, if the global maxima location (where the highest concentration was detected by all the robots so far) remains unchanged after the robots have moved 5 more steps, the robots will consider that they have been trapped in a local extremum area (where the concentration is higher than that of the surrounding area). Then, the robots will try to escape from the local extremum area by using a random divergence strategy to explore a larger area and find the plume again. Once a higher concentration value is detected, the robots will resume the plume tracking subtask.
- (3) Source declaration: During the plume tracking subtask, if any of the robots detects a concentration greater than the threshold of source declaration C_d , the robots will terminate the source localization process and consider that the last global maxima location is the source location. The source location determined by the robots will be compared to the actual source location to determine whether the source localization task is successful.

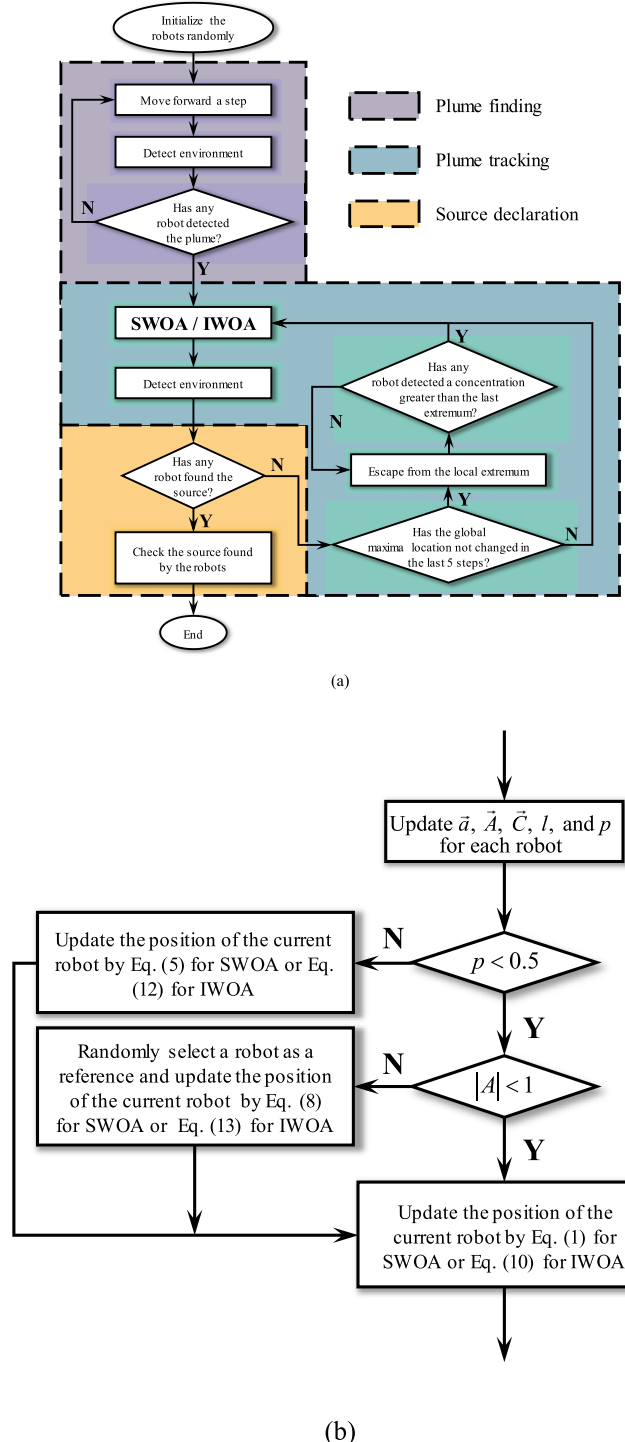


Fig. 1. Framework and procedure of the two WOA-based multi-robot olfaction methods: (a) Overall process; (b) the details of the SWOA and IWOA algorithms.

These two multi-robot olfaction methods also integrate an obstacle avoidance algorithm, in which walls and other types of obstacles, such as desks and occupants, are not treated differently. During the plume finding process, if a robot collides with an obstacle, it will turn like light reflecting off a mirror plane. During the plume tracking process, if a robot collides with an obstacle, it will move along the direction parallel to the surface of the obstacle. The details of this obstacle avoidance algorithm can be found in our previous research [24].

In practical applications, the SWOA and IWOA methods can be compiled into source localization applications and integrated into a

multi-robot source localization system. When the application is launched, multiple robots work together to find the particle plume, track the particle plume, and finally determine the location of the particle source. The whole process can be done autonomously without human intervention. In normal times, multiple robots can patrol in an indoor environment with random or preset routes to assist with routine maintenance and management. In emergency situations, such as bioterrorist attacks, multiple robots can be quickly deployed on-site to assist with emergency response. Whether in normal times or emergency situations, the robots can issue an early warning in time when they detect a concentration higher than the preset plume tracking threshold and report the source location after finally confirming the source location. It is worth noting that the multi-robot source localization system is an open platform. Based on this platform, not only the applications for locating particle sources can be continuously improved and updated, but other applications, such as the applications for locating gas sources, can also be installed.

2.2. SWOA for plume tracking

The WOA is an optimization algorithm inspired by the special hunting behavior of humpback whales and is executed iteratively to find the best solution of an optimization problem. It has been proven that the WOA algorithm has a superior exploration capability and perform better than the PSO algorithm while escaping from local maxima in multimodal function tests [37]. More details of this algorithm can be referred to in Ref. [37].

Based on the basic principle of the WOA, we developed the SWOA that does not rely on airflow information for tracking the plume. The SWOA uses the concentration as a fitness function and treats the robots and the particle source as whales and prey, respectively. The robots mimic the hunting behavior of humpback whales and locate the source by encircling and approaching the global maxima location. In addition, the robots will explore a larger area by moving away from a randomly selected robot to increase the likelihood of finding the source. The SWOA simulates the hunting behaviors of humpback whales by three operators, namely, the encircling prey operator, bubble-net attacking operator and searching for prey operator, which are briefly introduced in the following sections.

2.2.1. Encircling prey operator

In this operator, the global maxima location is assumed to be the location of the source or a location close to the source, and all robots will approach this location and update their coordinates in time to locate the source. This behavior of the robots is described by the following equations:

$$\vec{X}(t+1) = \vec{X}^*(t) - \vec{A} \cdot \vec{D} \quad (1)$$

$$\vec{D} = |\vec{C} \cdot \vec{X}^*(t) - \vec{X}(t)| \quad (2)$$

where $\vec{X}(t+1)$ and $\vec{X}(t)$ are the position vectors of a robot at moments $t+1$ and t , respectively; $\vec{X}^*(t)$ is the position vector of the global maxima location and to be updated in every iteration if a higher concentration is detected; $||$ represents the absolute value; “ \cdot ” represents an element-by-element multiplication; and \vec{A} and \vec{C} are coefficient vectors, which are represented by the following equations:

$$\vec{A} = 2\vec{a} \cdot \vec{r}_1 - \vec{a} \quad (3)$$

$$\vec{C} = 2\vec{r}_2 \quad (4)$$

where \vec{a} linearly decreases from 2 to 0 over time and \vec{r}_1 and \vec{r}_2 are random vectors in the range [0,1].

Fig. 2 illustrates the principle of Eq. (1) in a 3D space. A robot's current position is (X, Y, Z) , and the current global maxima location is (X^*, Y^*, Z^*) . By defining the random vectors \vec{A} and \vec{C} , Eq. (1) allows

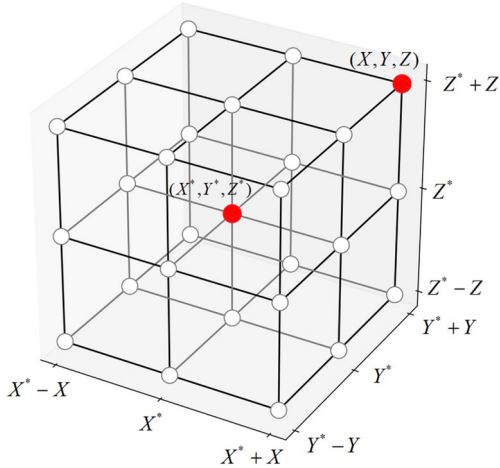


Fig. 2. Schematic of the encircling prey operator (Adapted from Ref. [37]).

the robots to update their positions around the current global maxima location and encircle it.

2.2.2. Bubble-net attacking operator

The bubble-net attacking operator simulates the bubble-net feeding behavior of humpback whales. Two mechanisms of bubble-net feeding, namely, shrinking encircling and spiral updating, are modeled as follows:

1. Shrinking encircling: This mechanism is modeled by Eqs. (1) and (3). During the plume tracking process, \vec{A} linearly decreases from 2 to 0, resulting in a gradual decrease in the fluctuation amplitude of \vec{A} . As the number of iterations increases, $\vec{X}(t+1)$ will gradually approach $\vec{X}^*(t)$, and the robots will also be closer to each other, thus shrinking the encirclement.
2. Spiral updating: As shown in Fig. 3, the distance \vec{D}' between a robot and the current global maxima location is first calculated to mimic the helix-shaped movement of a humpback whale. Then, the position of the robot is updated using a spiral equation (Eq. (5)). This mechanism is modeled as follows:

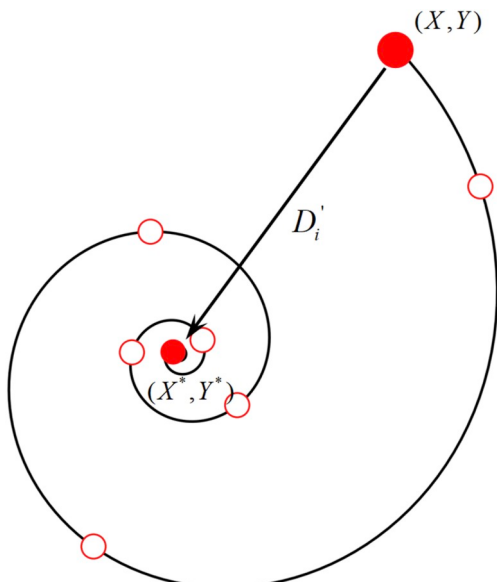


Fig. 3. Trajectory of a robot that moves from (X, Y) to (X^*, Y^*) according to the mechanism of spiral updating (Adapted from Ref. [37]).

$$\vec{X}(t+1) = \vec{D}' \cdot e^{bl} \cdot \cos(2\pi l) + \vec{X}^*(t) \quad (5)$$

$$\vec{D}' = |\vec{X}^*(t) - \vec{X}(t)| \quad (6)$$

where b is a constant for defining the shape of the logarithmic spiral and l is a random number in the range of $[-1, 1]$.

In the bubble-net feeding process, the humpback whales swim along a spiral path while shrinking the encirclement. To simulate this process, the robots randomly select the mechanisms of shrinking encircling and spiral updating with a 50% probability for each mechanism when updating their positions. This process is modeled as follows:

$$\vec{X}(t+1) = \begin{cases} \vec{X}^*(t) - \vec{A} \cdot \vec{D} & p < 0.5 \\ \vec{D}' \cdot e^{bl} \cdot \cos(2\pi l) + \vec{X}^*(t) & p \geq 0.5 \end{cases} \quad (7)$$

where p is a random number in the range of $[0, 1]$.

2.2.3. Search for prey operator

The bubble-net attacking operator uses the variation in \vec{A} to shrink the encirclement and approach the current global maxima location. Similarly, the search for prey operator also uses the variation in \vec{A} to search for prey (plume of particles) and execute a global search. When $|\vec{A}|$ is equal to or greater than 1, the SWOA forces a robot to update its position by taking the position of a randomly selected robot (including itself) as the reference position and lets the robot move far away from the selected robot. This operator allows the robots to search more area than just moving toward the global maxima location (Fig. 4). The mathematical model is as follows:

$$\vec{X}(t+1) = \vec{X}_{rand}(t) - \vec{A} \cdot \vec{D}'' \quad (8)$$

$$\vec{D}'' = |\vec{C} \cdot \vec{X}_{rand}(t) - \vec{X}(t)| \quad (9)$$

where \vec{X}_{rand} is the position vector of a randomly chosen robot.

2.3. IWOA for plume tracking

For the cases where the robots can be equipped with anemometers, we further developed the IWOA that uses both concentration and airflow information for plume tracking. This algorithm adds an upwind term to the SWOA to help the robots escape from a local extremum area more efficiently and find the source more quickly. Specifically, Eq. (1) in the SWOA is modified to Eq. (10) as follows:

$$\vec{X}(t+1) = \vec{X}^*(t) - \vec{A} \cdot \vec{D} + \vec{V}^u(t) \quad (10)$$

where $\vec{V}^u(t)$ is the upwind term, which is defined as follows:

$$\vec{V}^u(t) = \begin{cases} -L_{max} \cdot \vec{V}^s(t) / |\vec{V}^s(t)| & |\vec{V}^s(t)| \geq V_{th} \\ L_{max} \cdot \vec{V}_{rand} & |\vec{V}^s(t)| < V_{th} \end{cases} \quad (11)$$

where L_{max} is the maximum step length of the robots; V_{th} is the measurement threshold of the anemometer; $\vec{V}^s(t)$ is the airflow velocity at moment t ; $|\vec{V}^s(t)|$ is the length of $\vec{V}^s(t)$; and \vec{V}_{rand} is a random unit vector. If the airflow velocity is lower than the measurement threshold of the anemometer, the wind direction detected by the anemometer is unreliable for plume tracking. Therefore, we set the direction of the upwind term to be a random vector so that the robots can explore a larger area.

In addition, Eqs. (5) and (8) in the SWOA are modified to Eqs. (12) and (13), respectively, as follows:

$$\vec{X}(t+1) = \vec{D}' \cdot e^{bl} \cdot \cos(2\pi l) + \vec{X}^*(t) + \vec{V}^u(t) \quad (12)$$

$$\vec{X}(t+1) = \vec{X}_{rand}(t) - \vec{A} \cdot \vec{D}'' + \vec{V}^u(t) \quad (13)$$

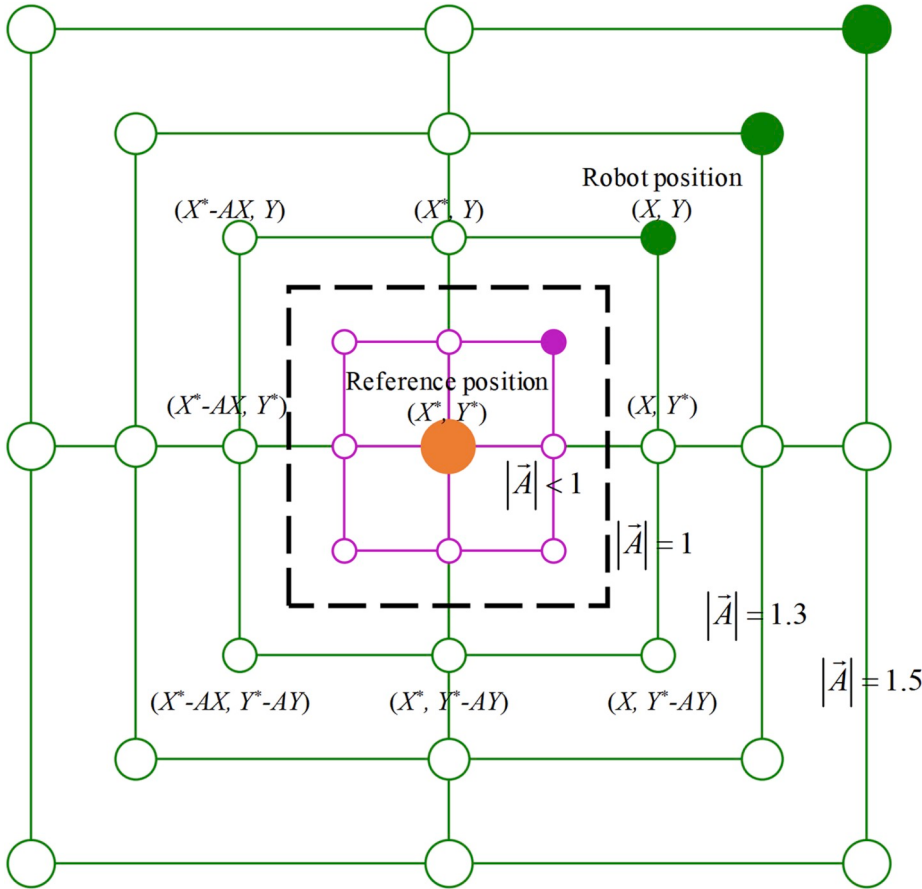


Fig. 4. An example of the search for prey operator when \vec{C} is a zero vector. (X^*, Y^*) is the position of the randomly selected robot. When $|\vec{A}|$ is equal to or greater than 1, the new position updated by Eq. (5) will be further away from a randomly selected robot (green area) rather than closer to the global maxima location (magenta area) (Adapted from Ref. [37]). (For interpretation of the references to colour in this figure legend, the reader is referred to the Web version of this article.)

3. Case study

3.1. Validation procedure

As shown in Fig. 5, the presented source localization methods (SWOA and IWOA methods) were validated by combining CFD simulations with laboratory experiments. First, airflow velocity profiles and particle concentrations in an experimental chamber were measured. Then, the measurements were compared with the CFD simulation results for the chamber. After the feasibility of the CFD method was validated, the CFD method was used to simulate four typical particle dispersion scenarios. Finally, the simulation results were exported as virtual environments to test the presented source localization methods and their comparison methods (SPSO and IPSO methods) on the Python platform.

3.2. Laboratory measurements

The laboratory measurements were conducted in an experimental chamber ($6 \text{ m} \times 4.5 \text{ m} \times 3 \text{ m}$) with mixing ventilation (Fig. 6). Air was supplied from a diffuser on the ceiling of the chamber and exhausted through an outlet on the top of the right wall. Mono-dispersed $2.5 \mu\text{m}$ particles (1050 kg/m^3) were continuously released in the air supply duct for 100 s.

The airflow velocity profiles were measured by hot-sphere anemometers (SENSOR, HT400; accuracy: $\pm 0.03 \text{ m/s}$) at a time interval of 2 s. A total of six sampling lines of airflow velocity (L1–L6) were set in the chamber. For each sampling line, seven sampling points were set, starting from a height of 0.35 m to a height of 2.45 m with an interval of

0.35 m (Fig. 6). The particle concentrations were measured at P1–P5 using optical particle counters (TSI, Aerotrak 8220; counting efficiency: $100\% \pm 10\%$ at $0.45 \mu\text{m}$ and greater) at an interval of 10 s (Fig. 6). The particle dispersion experiments were repeated three times under the same conditions to obtain the standard deviation. To facilitate the comparison of the particle concentrations obtained by the experiment and simulation, all measurements and simulation results were first normalized by dividing a reference concentration C_{ref} and then compared to each other. The reference concentration C_{ref} was the average of the concentrations at the five sampling points (P1–P5) for experiments and simulations for each sampling interval. For more details, please refer to our previous study [26].

3.3. Numerical method and validation

The distribution of airflow and the dispersion of particles were simulated by adopting unsteady Reynolds-averaged Navier-Stokes (URANS) with the renormalization group k-e (RNG k-e) turbulence model. The RNG k-e model has been successfully used to simulate airflow and contaminant distributions in different enclosed spaces [42–44]. Zhang et al. [45] summarized the corresponding governing transport equations of the RNG k-e turbulence as follows:

$$\frac{\partial(\rho\varphi)}{\partial t} + \nabla \cdot (\rho\vec{u}\varphi - \rho\Gamma_{\varphi,\text{eff}}\nabla(\varphi)) = S_\varphi \quad (14)$$

where φ represents variables such as time-averaged velocity components, enthalpy, contaminant concentration, and turbulent parameters; $\Gamma_{\varphi,\text{eff}}$ is the effective diffusion coefficient; and S_φ is the source term. Detailed information about the terms and coefficients for different

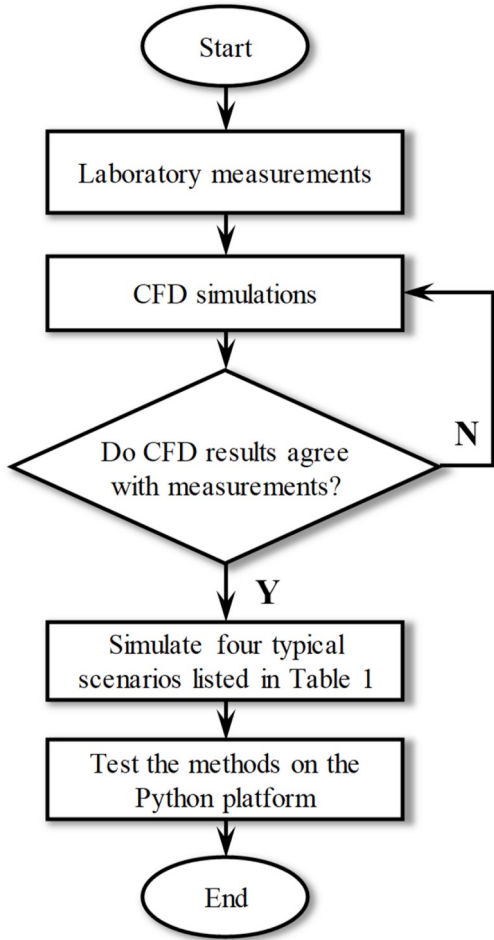


Fig. 5. Validation procedure of the presented source localization methods.

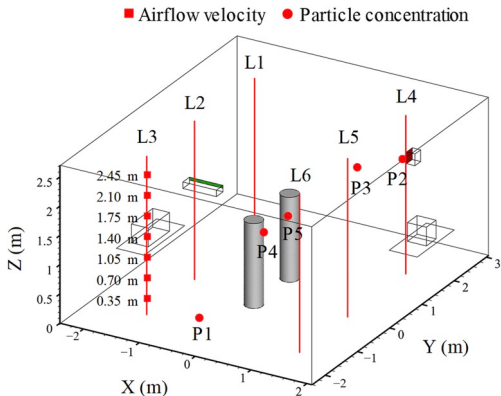


Fig. 6. The experimental chamber with six sampling lines (L1–L6) of airflow velocity, five sampling points (P1–P5) of particle concentration (P1 (0.0 m, -2.35 m, 0.59 m), P2 (2.05 m, 0.63 m, 2.55 m), P3 (0.0 m, 2.72 m, 1.3 m), P4 (0.0 m, -0.35 m, 1.3 m), P5 (0.0 m, 0.35 m, 1.3 m)).

variables can be found in Ref. [45]. For investigating indoor particle dispersion, an Eulerian model was employed and integrated with gravity settling effects into the concentration equation, which can be written as:

$$\frac{\partial(\rho C)}{\partial t} + \nabla \cdot \left(\rho (\vec{u} + \vec{V}_S) C - \frac{\mu_{eff}}{\sigma_C} \nabla C \right) = S_C \quad (15)$$

where C is the concentration of contaminant; S_C is the release rate of the particle source; σ_C is the turbulent Schmidt number, which is 1.0

[46]; and \vec{V}_S is the settling velocity of particles [47]. The magnitude of the particle settling velocity can be expressed as:

$$|\vec{V}_S| = \left[\frac{4}{3} \frac{g \cdot d_p}{C_D} \frac{\rho_p - \rho}{\rho_a} \right]^{1/2} \quad (16)$$

where d_p is the diameter of the particle, C_D is the drag coefficient, and ρ_p is the density of the particle. It should be noted that the drift flux model assumes that the turbulence is not affected by particles and treats the solid particles as a continuum. To satisfy these assumptions, the particles should fall under the scale of the Kolmogorov micro airflow field, and the volume fraction of particles should be less than 10^{-6} . Holmberg et al. [46] verified these assumptions in common residence and commercial buildings.

A second-order upwind scheme was used for all the variables except pressure. PRESTO! was applied to discretize pressure levels, and the SIMPLE algorithm was applied for coupling the pressure and momentum. The residual values were less than 10^{-6} for energy and 10^{-4} for other variables. The influence of the manikin buoyancy was calculated by the Boussinesq approximation. Grid independence was checked in Ref. [26] by comparing different grid resolutions (247,000, 500,000, and 1,000,000), and a resolution of 500,000 grids was proven to be enough for this simulation [48]. The surface temperature was also controlled to simulate thermal boundaries. The boundary conditions of the manikins and walls were set as heat fluxes. For more details of the boundary settings, please refer to Ref. [26].

Fig. 7 illustrates a comparison of airflow velocity profiles between the measurements and the CFD simulations. The error bars mean the measurement errors caused by the accuracy of the anemometers (0.03 m/s). The locations of the sampling lines (L1–L6) can be found in **Fig. 6**. As shown in **Fig. 7**, the simulation results agree well with the measurements because of the mixing effect. However, the clear discrepancies at L5 and L6 at heights below 0.6 m should not be ignored.

For the sake of brevity, **Fig. 8** presents a comparison of the particle concentrations at three representative points P1–P3 (**Fig. 6**) between the measurements and simulation results. For P2 and P3, the simulation results are consistent with the measurements. However, a significant discrepancy can be found at P1 because this point was in the recirculation region where concentration fluctuated significantly.

According to the results shown in **Figs. 7 and 8**, it can be concluded that URANS for predicting the airflow distribution and the Eulerian drift flux model for predicting particle dispersion can generate reasonable simulation results. Thus, it is feasible to use these models to simulate typical scenarios of particle dispersion in the chamber.

3.4. Case setup

After the CFD validation, we further simulated four typical scenarios (**Table 1**) and exported them as virtual environments to test the source localization methods. All the CFD models were set up based on the above-mentioned experimental chamber (**Fig. 6**). Two types of typical time-varying particle sources, a decaying source (e.g., the bioaerosol released from a small spray device) [27] and a periodic source (e.g., the respiratory activities of patients infected by SARS or H1N1-A) [28], were considered, and their release rates over time are described as follows:

$$M_D(t) = M_0 e^{\frac{t}{100}} \quad (17)$$

$$M_P(t) = \begin{cases} M_0 \sin\left(\frac{t}{2.5}\pi\right), & 6n < t < 2.5 + 6n \\ 0 & \text{otherwise} \end{cases} \quad (18)$$

where $M_D(t)$ and $M_P(t)$ are the release rates of the decaying source and periodic source at moment t , respectively; M_0 is a constant release rate; and n is an integer.

For each type of source, two ventilation modes, mixing ventilation

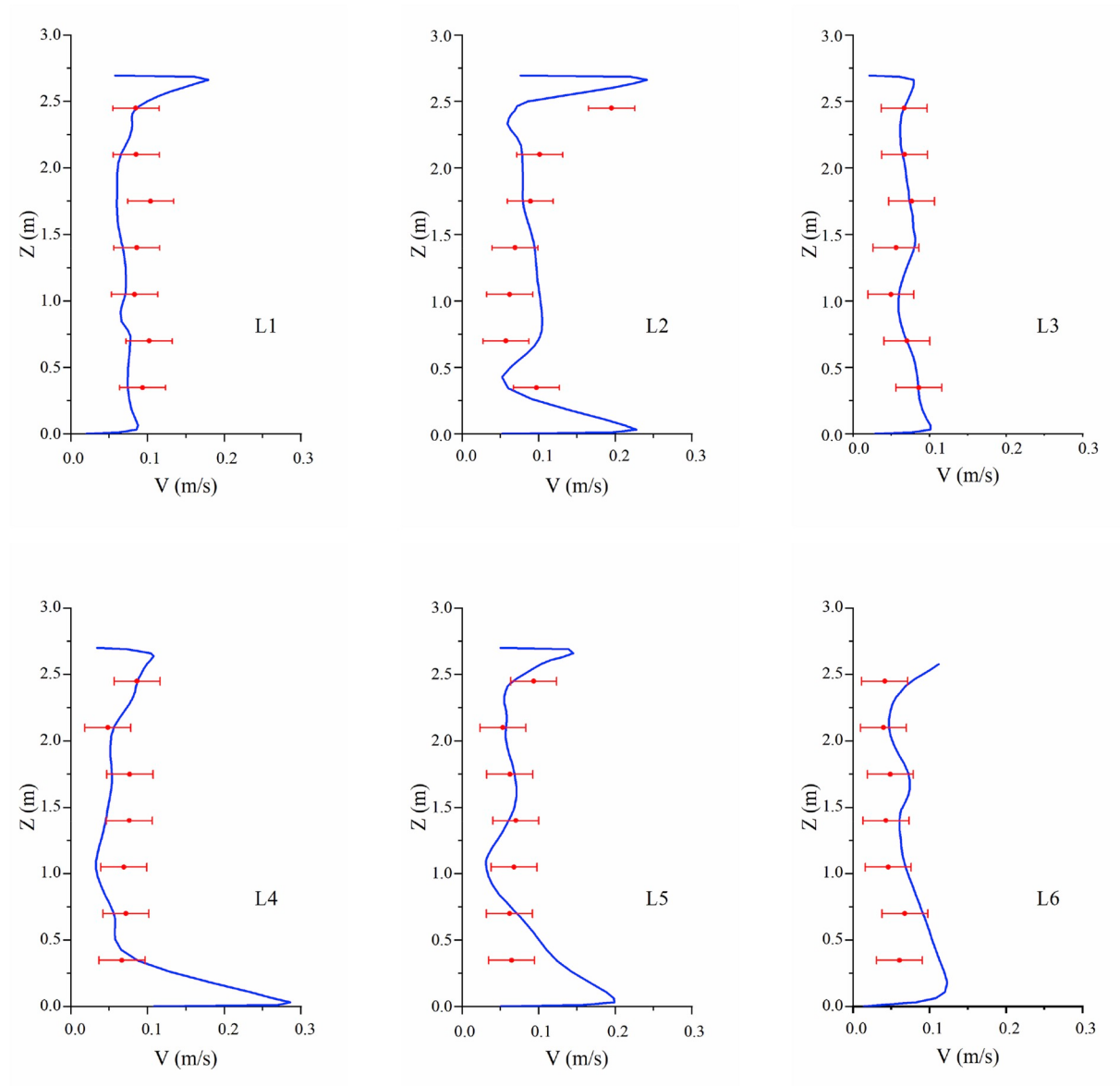


Fig. 7. Comparison of the measured (red symbols) and predicted (blue lines) airflow velocity profiles at different locations. (For interpretation of the references to colour in this figure legend, the reader is referred to the Web version of this article.)

and displacement ventilation, were simulated. The positions of the inlet and outlet for each ventilation mode are shown in Fig. 9. The ventilation rate of both ventilation modes was set to 3.2 ACHs. For all four scenarios, two cylinders with a diameter of 0.3 m and a height of 1.5 m were set as manikins in the chamber. The manikins were fully coated with electric heaters, which provided a constant heat flux of 90 W (Fig. 9).

The SWOA and IWOA methods were validated in the above four scenarios and compared with the SPSO and IPSO methods, respectively. For the comparison of the SWOA and SPSO methods, each method was tested by 100 independent experiments in each scenario, and a total of 800 experiments were conducted. For the comparison of the IWOA and IPSO methods, three different measurement thresholds of anemometers (0.1 m/s, 0.05 m/s, 0.01 m/s) were compared in each scenario. Thus, a total of 2400 experiments were conducted.

For fair comparison, all the source localization methods used the same plume finding strategy, obstacle avoidance algorithm and other settings. In each experiment, 6 robots were used to locate the source. To reduce the influence of movements of the robots on the airflow and

particle concentration, the maximum linear speed and the maximum step length of each robot were set to 0.3 m/s and 0.3 m, respectively, by referring to the real robot experiments in our previous studies [23,31]. Therefore, the time period for each robot to move to the next location was approximately 1 s. The time period for each robot to determine the next location was not taken into account, because this process can be done in an instant by the computer carried by each robot. In addition, for the purpose of simplification, the real characteristics of sensors, such as response time and measurement error, were not considered. The threshold of plume finding C_t was a constant value of $50 \mu\text{g}/\text{m}^3$ for each scenario, while the threshold of source declaration C_d was the average concentration in the area within 0.5 m of the source. In addition, the source localization task was considered successful when the source was found by the robots within 100 steps and the distance between the source location determined by the robots and the actual source location was less than 0.5 m.

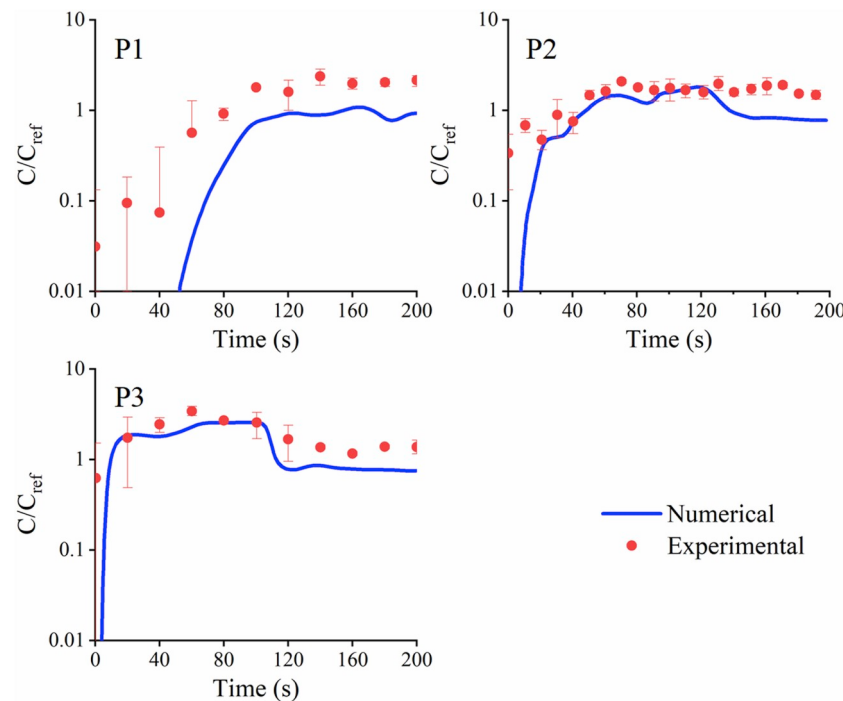


Fig. 8. Comparison of experimental (red symbols) and numerical particle concentrations (blue lines) at different positions. (For interpretation of the references to colour in this figure legend, the reader is referred to the Web version of this article.)

Table 1
Validation case settings.

Scenario No.	Source type	Ventilation mode	Source position (x, y, z) (m)
Dec_Mix	Decaying	Mixing	(0.0, 1.5, 0.8)
Dec_Dis	Decaying	Displacement	(0.0, 1.5, 0.8)
Per_Mix	Periodic	Mixing	(0.0, -0.3, 1.3)
Per_Dis	Periodic	Displacement	(0.0, -0.3, 1.3)

4. Results and discussion

4.1. Airflow and particle distributions

Fig. 10 shows the airflow distributions of the mixing and displacement ventilation modes. For the mixing ventilation mode, a distinct airflow was ejected from the inlet, and the airflow velocity was above 1 m/s. After the airflow reached the wall, a vortex was formed between the wall and the right manikin, and a thermal plume was generated around the manikins (Fig. 10 (a)). For the displacement ventilation

mode, no distinct airflow was formed, and the airflow velocity was below 0.5 m/s. A thermal plume was also noticeable around the manikins (Fig. 10 (b)).

Fig. 11 shows the particle distributions of the four scenarios after the source released for 60 s. For the Dec_Mix and Dec_Dis scenarios, isolated local extremum areas were formed away from the source. For the Per_Mix scenario, a local extremum area was formed above the source, and the concentration of this area was lower than that around the source. For the Per_Dis scenario, a continuous plume was observed, and no isolated local extremum area was formed.

4.2. Source localization results and comparison

4.2.1. Source localization without airflow information

Fig. 12 shows the source localization process of the SWOA method for the Per_Mix scenario in a typical successful experiment (a video of this experiment is provided in the supplemental material). The typical successful experiment refers to a successful experiment in which the trajectories of robots can fully illustrate the basic principle of the SWOA

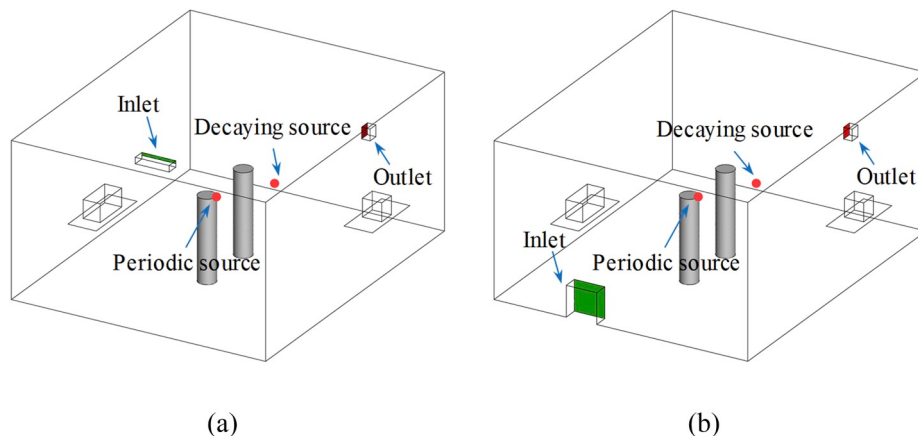


Fig. 9. Experimental chamber with two typical ventilation modes: (a) mixing ventilation and (b) displacement ventilation.

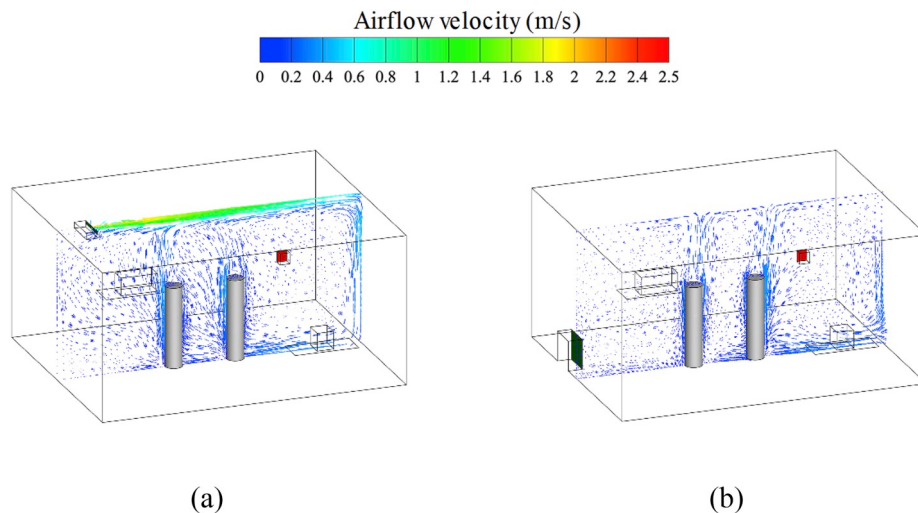


Fig. 10. Airflow distributions on the YZ plane ($X = 0.0\text{ m}$): (a) mixing ventilation mode; (b) displacement ventilation mode.

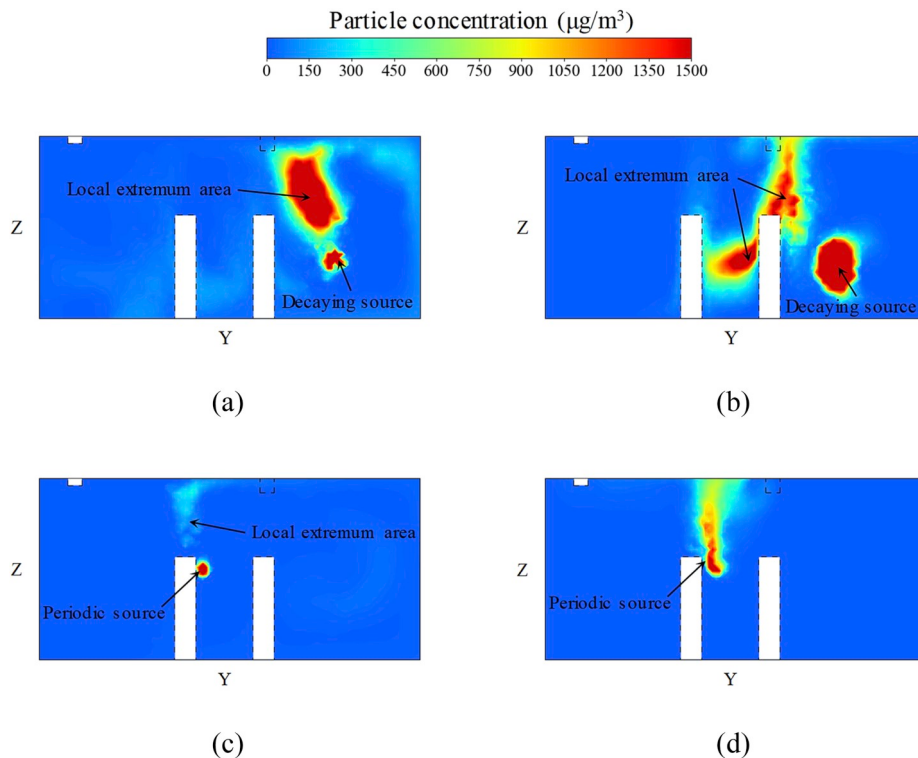


Fig. 11. Particle distributions on the YZ plane ($X = 0.0\text{ m}$) at 60 s in scenario: (a) Dec_Mix; (b) Dec_Dis; (c) Per_Mix; (d) Per_Dis.

method, and the source localization time was also close to the average source localization time for the Per_Mix scenario. After particles were released from the source (at 0 s), the six robots (R1–R6) were initialized at random positions in the chamber at 1 s (Fig. 12 (a)) and used a random divergence strategy to find the plume of particles. At 22 s, R6 first discovered the plume (Fig. 12 (b)). Subsequently, R1–R6 tracked the plume and moved toward the higher concentration area using the SWOA.

Supplementary video related to this article can be found at <https://doi.org/10.1016/j.buildenv.2019.106413>.

During the plume tracking subtask, the robots became trapped in local extremum areas twice. Taking the second time as an example, the global maxima location had not been updated for 5 s at 56 s (Fig. 12 (c)), so the robots determined that they were trapped in a local extremum area. Then, the random divergence strategy was used to escape

from this area. At 58 s, R2 detected a higher concentration, and R1–R6 started to track the plume again (Fig. 12 (d)).

At 65 s, the robots gathered near the source (Fig. 12 (e)), but they failed to declare the source as no particle was released from the periodic source at that moment. At 67 s, R6 detected a concentration higher than the source declaration threshold C_d (Fig. 12 (f)), and all the robots terminated the source localization process. The source location determined by the robots was 0.27 m away from the actual source location. Therefore, the source localization task was considered successful.

Fig. 13 shows the trajectories of the robots in the above experiment. As shown in Fig. 13 (a), the robots first moved along straight lines according to the random divergence strategy. After the plume was found, the robots moved toward the global maxima location and tracked the plume with the encircling prey and spiral updating mechanisms. The movement trend of the robots is indicated by the two red

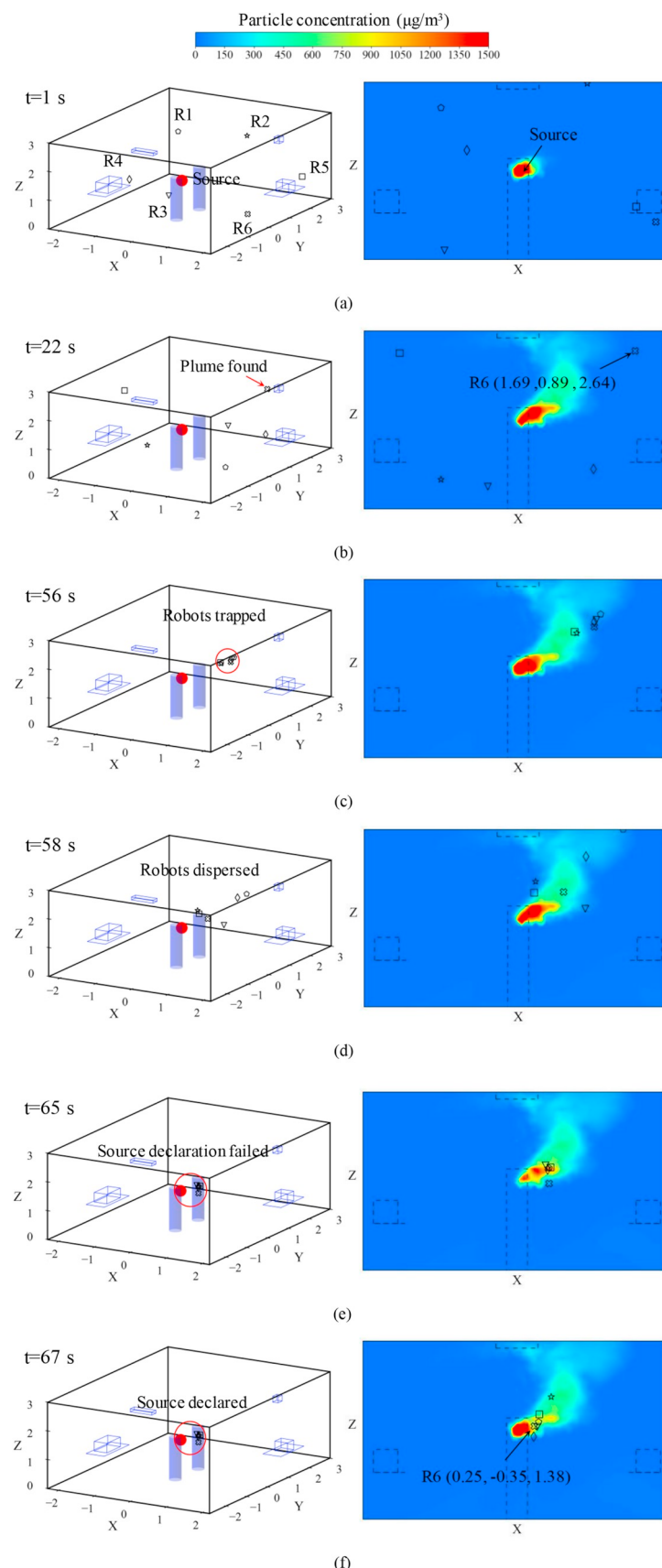


Fig. 12. Source localization process (3D plot and projection onto the plane $Y = -0.3 \text{ m}$) of the SWOA method for the Per_Mix scenario in a typical successful experiment.

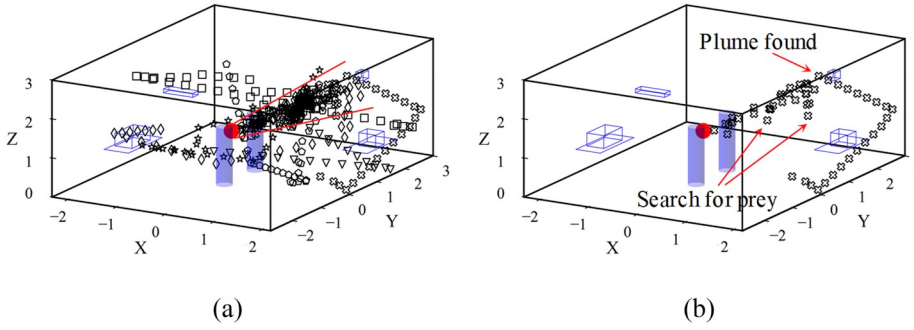


Fig. 13. The trajectories of the robots in the successful experiment for the Per_Mix scenario: (a) trajectories of R1–R6; (b) trajectory of R6.

lines in Fig. 13 (a). This trend shows that the shrinking encircling mechanism made the robots move closer to each other when approaching the source. Fig. 13 (b) shows the trajectory of R6. The search for prey operator enabled R6 to explore a larger area when approaching the source. However, this operator also caused R6 to leave the plume area, but R6 soon switched to the plume tracking subtask again because another robot detected a new global maxima location in the plume.

Fig. 14 shows the change in the global maxima location and the distance between the global maxima location and the actual source location. After the plume was found, the global maxima location was updated during the plume tracking subtask. As shown in Fig. 14 (a), the global maxima location remained unchanged in two local extremum areas. Taking the second local extremum area as an example again, the distance to the source remained unchanged from 51 s to 56 s, as shown in Fig. 14 (b). Then, the robots used the random divergence strategy to escape the local extremum area and found a higher concentration at 58 s. It should also be noted that the distance fluctuated between 32 s and 43 s, indicating that the robots could not continuously track the plume using only concentration information during this period.

The performances of the methods were evaluated by two indices of success rate (SR) and average localization time (ALT). The SR is the number of successful experiments divided by the number of total experiments for each scenario, which reflects the robustness of the source localization method. The ALT is the average of the localization times of the experiments in each scenario, which reflects the efficiency of the source localization methods.

Fig. 15 shows the SR and ALT results of the SPSO and SWOA methods in the four typical scenarios (Table 1) without using airflow information. The credibility of these results is supported by statistical tests (see Appendix A for details). In the cases of the decaying source, the SWOA method performed slightly worse than the SPSO method, as shown by a slightly lower SR value (2% lower for case Dec_Dis) and higher ALT values (5.10 s and 6.13 s higher for cases Dec_Mix and

Dec_Dis, respectively) for the SWOA method. In the cases of the periodic source, the SWOA method performed significantly better than the SPSO method, with much higher SR values (28% and 30% higher for cases Per_Mix and Per_Dis, respectively) and lower ALT values (14.30 s and 13.63 s lower for cases Per_Mix and Per_Dis, respectively). Overall, by comparing these two methods in all four scenarios, we concluded that the performance of the SWOA method was significantly better. The average SR (66%) was significantly higher than that of the SPSO method (52%), and the average ALT (65.48 s) was slightly lower than that of the SPSO method (69.65 s).

Further analysis based on the source types reveals that the performance of both the SPSO and SWOA methods declined (with decreases in SR and increases in ALT) in the cases with the periodic source compared to their performance in the cases with the decaying source. The performance of the SPSO method decreased significantly in the cases with the periodic source, and the SR values in the Per_Mix and Per_Dis scenarios were only 41% and 26%, respectively, which were too low to meet the requirements of practical applications. In contrast, the SWOA method only exhibited a slight decrease in performance, and the SR values in the Per_Mix and Per_Dis scenarios were 69% and 56%, respectively, which were still above an acceptable level.

In summary, for source localization without using airflow information, we can conclude that the SWOA method generally performed better than the SPSO method in four typical scenarios. Although the SWOA method performed slightly worse than the SPSO method in the cases with the decaying source, the SWOA method outperformed significantly in the cases with the periodic source. The performance of both methods declined in the cases with the periodic source, and the SR values of the SPSO method were too low to meet the requirements of practical applications, while those values of the SWOA method were still above an acceptable level.

The anemometers currently available on the market are expensive and bulky. Based on this study, the SWOA method without using

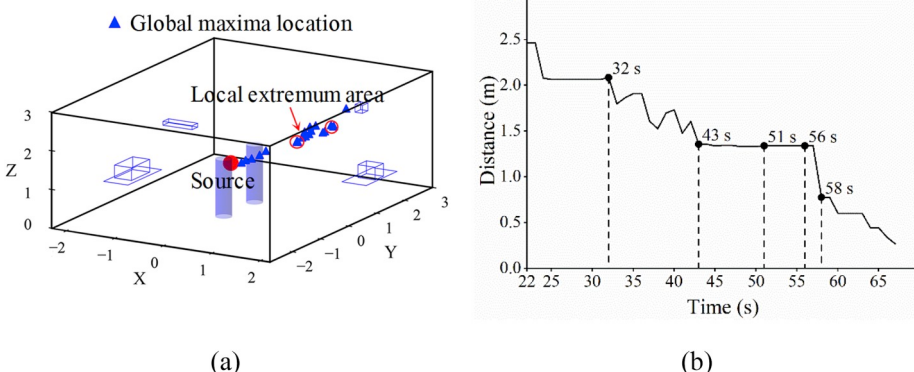


Fig. 14. The change in the global maxima location in the successful experiment for the Per_Mix scenario: (a) 3D plot; (b) variation in the distance between the global maxima location and the actual source location.

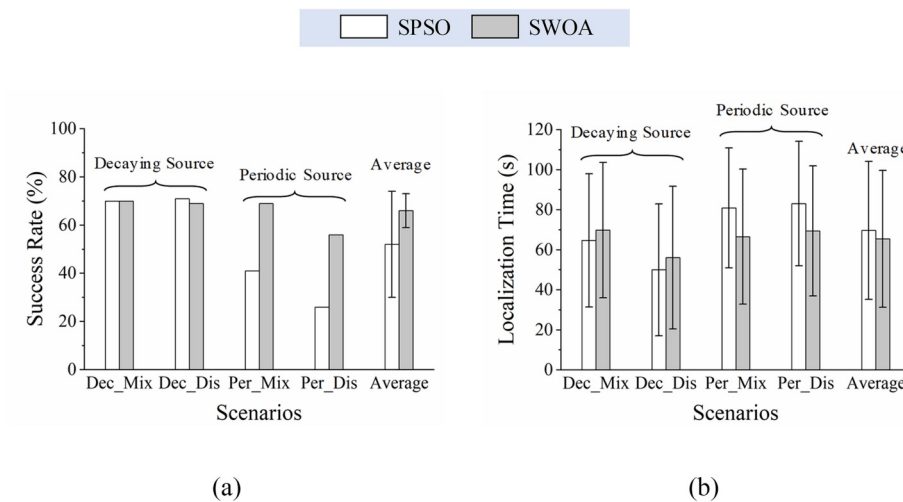


Fig. 15. Source localization results for the SPSO and SWOA methods in four typical scenarios without using airflow information: (a) SR (b) ALT (Dec_Mix: decaying source & mixed ventilation, Dec_Dis: decaying source & displacement ventilation, Per_Mix: periodic source & mixed ventilation, Per_Dis: periodic source & displacement ventilation, Average: averages of the SR and ALT results in four typical scenarios; in each scenario, each method was tested with 100 numerical experiments, and a total of 800 numerical experiments were conducted).

airflow information shows excellent promise for the development of less expensive and more compact terrestrial robots for source localization. In addition, some recent attempts have been made to locate indoor contaminant sources by using NAVs [41]. Compared with terrestrial robots, NAVs are more flexible and have better obstacle avoidance capability. However, NAVs normally have limited load capacity and endurance and cannot be equipped with a bulky anemometer. The performance of the SWOA method without using airflow information also shows its application prospects in source localization by NAVs.

4.2.2. Source localization with airflow information

Fig. 16 shows the source localization process of the IWOA method for the Per_Mix scenario in a typical successful experiment (a video of this experiment is provided in the supplemental material). The typical successful experiment refers to a successful experiment in which the trajectories of robots can fully illustrate the basic principle of the IWOA method, and the source localization time was also close to the average source localization time for the Per_Mix scenario. After the robots departed from randomly distributed initial positions (Fig. 16 (a)), R4 first found the plume at 21 s (Fig. 16 (b)). Then, according to the IWOA, the six robots started to track the plume by moving upwind while searching for the higher concentration area.

Supplementary video related to this article can be found at <https://doi.org/10.1016/j.buildenv.2019.106413>.

During the plume tracking subtask, the robots became trapped in a local extremum area just once. At 23 s, R4 detected a relatively high concentration, and the global maxima location remained unchanged for 5 s until 28 s (Fig. 16 (c)). Therefore, the robots considered that they were trapped in a local extremum area and then successfully escaped from this area by using the random divergence strategy.

The source localization process was terminated at 33 s when R4 detected a concentration higher than C_d (Fig. 16 (d)). The task was successful because the source location determined by the robots was 0.34 m away from the actual source location. Note that the robots had not gathered at the end of the process. One reason may be the effects of the search for prey operator, which forced the robots to explore in the chamber by moving toward a randomly selected robot. Another reason may be that the upwind term made the source localization process more effective, and there was not enough time for the robots to shrink the encirclement.

Fig. 17 shows the trajectories of the robots in the above source localization process. As shown in Fig. 17 (a), the trajectories in the plume finding subtask are straight lines. Compared with the trajectories shown in Fig. 13 (a), the movement trend indicated by the red lines is more obvious. However, the shrinking encircling mechanism is not apparent

enough because the plume tracking subtask was terminated in just 12 s, and \vec{a} in the shrinking encircling mechanism only decreased slightly. As shown in Fig. 17 (b), the trajectory of R4 is nearly a straight line except for the deviations caused by the search for prey operator and the process of escaping from the local extremum area.

Fig. 18 demonstrates the historical positions of the global maxima location and the variation in their distance to the actual source location. The only local extremum area encountered by the robots in this experiment is shown in Fig. 18 (a). As shown in Fig. 18 (b), the distance remained the same between 23 s and 28 s, indicating that the robots had become trapped in a local extremum area. After the robots diverged in random directions, the distance decreased because a higher concentration was detected at 29 s. In contrast to the curve in Fig. 14 (b), the distance curve in Fig. 18 (b) does not fluctuate during the whole process of plume tracking, and this finding indicates that the upwind term can effectively help the robots continuously track the plume.

Fig. 19 shows the SR and ALT results for the IPSO and IWOA methods in the four typical scenarios (Table 1) when using anemometers with three different measurement thresholds. The credibility of these results is supported by statistical tests (see Appendix A for details). A comparison between the results in Figs. 19 and 15 shows that the use of airflow information significantly improved the performance of the robots in different scenarios. Both the IPSO and IWOA methods achieved high success rates, with a minimum SR value of 89% and a maximum SR value of 100%. In comparison, for the SWOA method implemented without using airflow information, the performance was only at an acceptable level, with maximum and minimum SR values of 70% and 56% and maximum and minimum ALT values of 69.79 s and 56.1 s, respectively (Fig. 15). For the IWOA method implemented using an anemometer with a measurement threshold of 0.05 m/s, the performance achieved a satisfactory level, with maximum and minimum SR values of 100% and 94% and maximum and minimum ALT values of 54.86 s and 35.38 s, respectively (Fig. 19).

Comparing the methods using airflow information to locate the source, the IWOA method has a slight advantage in SR, while the IPSO method has a slight advantage in localization efficiency. For the thresholds of 0.1 m/s, 0.05 m/s and 0.01 m/s, the average SR values of the IPSO method were 89%, 97%, and 96.75%, and those values of the IWOA method were 92%, 97.75, and 98.25%, respectively, indicating that the IWOA method had a slight advantage in SR. In addition, the average ALT values of the IPSO method were 47.20 s, 39.18 s and 41.52 s, and those values of the IWOA method were 45.28 s, 42.18 s, and 43.78 s, respectively, indicating that the IPSO method had a slight advantage in localization efficiency.

Further analysis indicated that the measurement threshold is also a key factor in the performance. In the cases with the decaying source

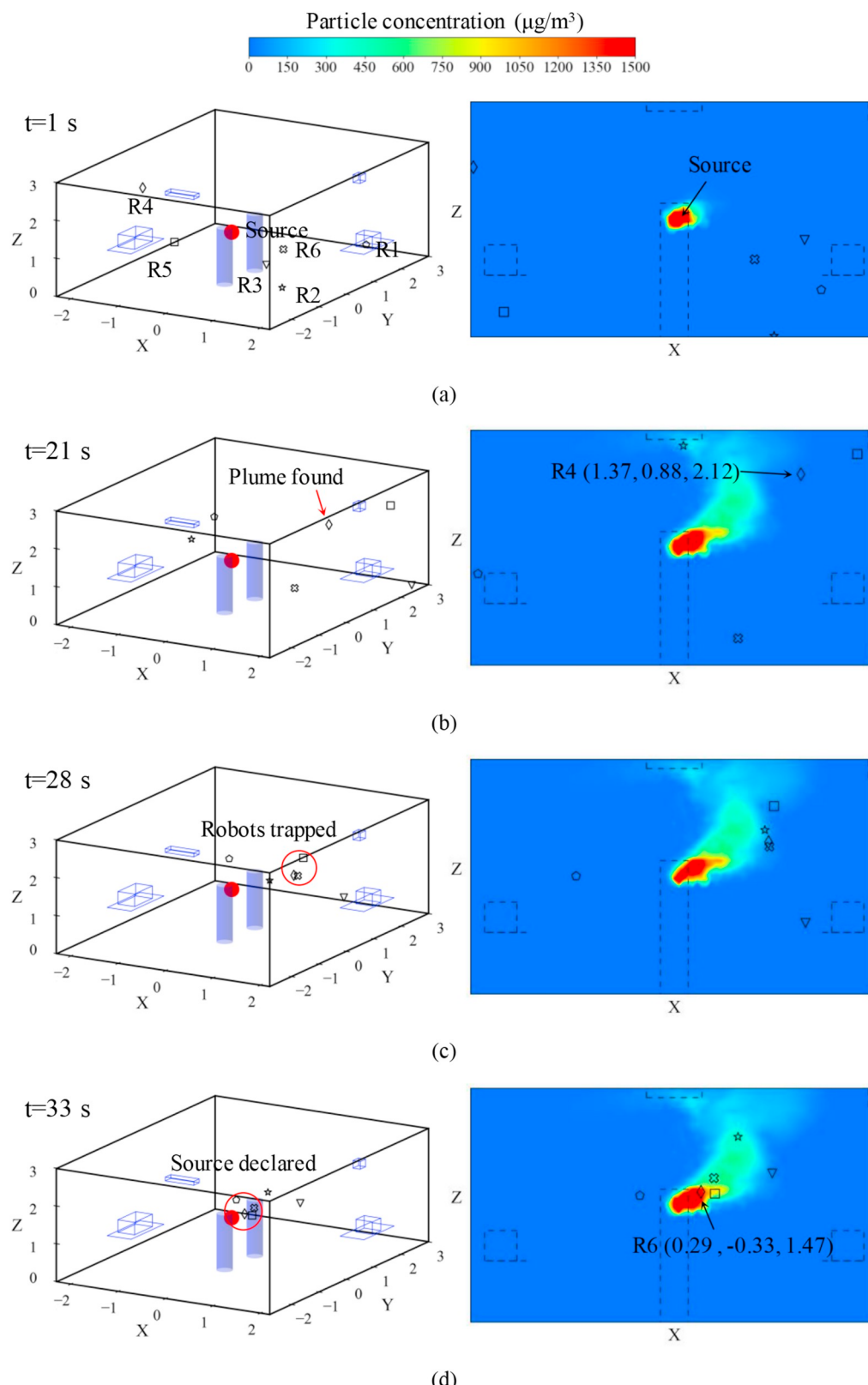


Fig. 16. Source localization process (3D plot and projection onto the $Y = -0.3$ m plane) of the IWOA method for the Per_Mix scenario in a typical successful experiment.

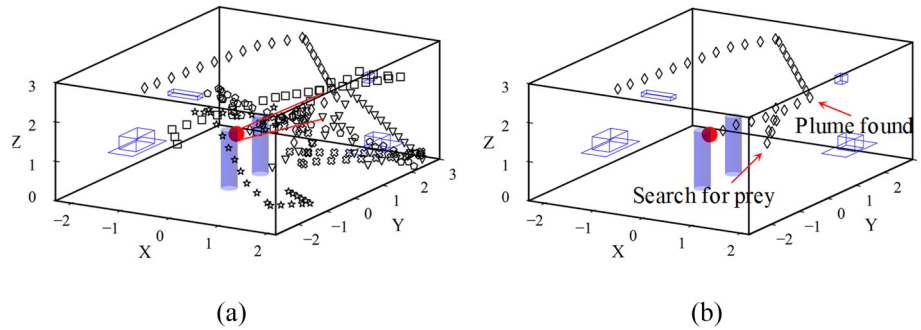


Fig. 17. The trajectories of the robots in the successful experiment for the Per_Mix scenario: (a) trajectories of R1–R6; (b) trajectory of R4.

(Dec_Mix and Dec_Dis), the performance of both methods significantly improved when the measurement threshold was reduced from 0.1 m/s to 0.05 m/s. In the Dec_Dis scenario, the SR values of the two methods increased from approximately 83%–98%. However, the improvement was not significant when the measurement threshold was further reduced from 0.05 m/s to 0.01 m/s. The above results show that the anemometer with a measurement threshold of 0.05 m/s was the most cost-effective choice in the cases with the decaying source. Unlike the decaying source, in the cases with the periodic source (Per_Mix and Per_Dis), a reduction in the measurement threshold did not significantly improve the performance of both the IPSO and IWOA methods, indicating that the anemometer with a measurement threshold of 0.1 m/s was the most cost-effective choice for the periodic source cases. The above results also indicate that, when the airflow velocity is lower than a certain level, the detected airflow information may have little effect on improving the performance of source localization.

In summary, using airflow information can significantly improve the performance of both the IPSO and IWOA methods and achieve high SRs. The IWOA method performed slightly better in terms of SR, while the IPSO method performed slightly better in terms of localization efficiency. In addition, this study was able to find the most cost-effective measurement thresholds of anemometers for a decaying source (0.05 m/s) and periodic source (0.1 m/s).

4.3. Limitations and future studies

For the four typical scenarios without using airflow information, the average SR of the SWOA method (66%) was only at an acceptable level, which means that the SWOA method still has a large room for improvement. In future study, we will further study whether the performance of the SWOA method can be improved by adjusting the

parameters of the algorithm, optimizing the obstacle avoidance algorithm, enhancing the robots' ability of escaping from local extremum areas, and improving the source declaration algorithm.

In this study, the SWOA and IWOA methods were validated by a large number of numerical experiments in four typical particle release scenarios simulated by CFD. Although numerical experiments have advantages in terms of time and cost requirements, it is still necessary to further validate the presented methods by real robot experiments in future study. The reasons are mainly threefold. First, due to the complexity of the indoor turbulence and particle dispersion, the errors between CFD results and experimental results are inevitable, which may have certain impact on the results of source localization and the impact should be evaluated in future study. Second, for simplification, the real characteristics of sensors, such as response time and measurement errors, were not considered in the numerical experiments. In future study, the influence of the real characteristics of sensors on the performance of source localization should be evaluated, and the methods for eliminating the delay of sensor measurements and reducing the measurement errors should also be investigated. Finally, the influence of robot movements on local airflow and particle concentration were neglected in numerical experiments. In real robot experiments, this influence should be considered and reduced, for example, by separating the robot and the sensor by a scalable rod or string.

We assumed that the indoor airflow field was in a steady state. This assumption applies to most indoor environments with mechanical ventilation. Nevertheless, indoor environments with dynamic airflows are widespread in real-world applications, such as those of natural ventilation and hybrid ventilation (a combination of mechanical and natural ventilation). In future study, we will try to extend the applications of the WOA-based methods to dynamic indoor environments.

This study focused on the issue of locating a single particle source in

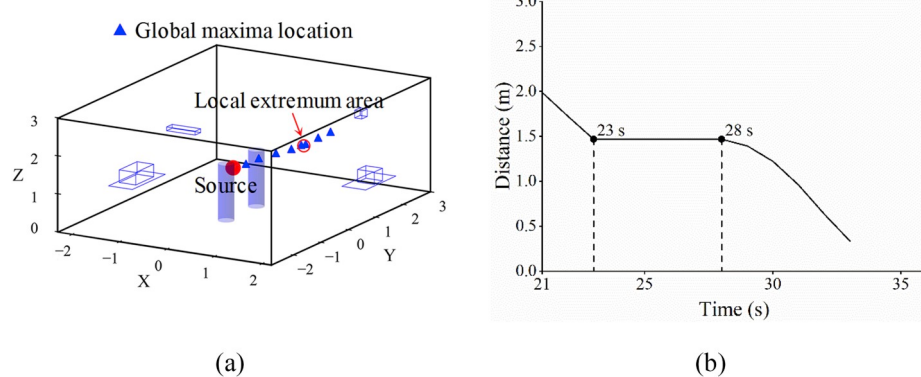


Fig. 18. The change in the global maxima location in the successful experiment for the Per_Mix scenario: (a) 3D plot; (b) variation in the distance between the global maxima location and the actual source location.

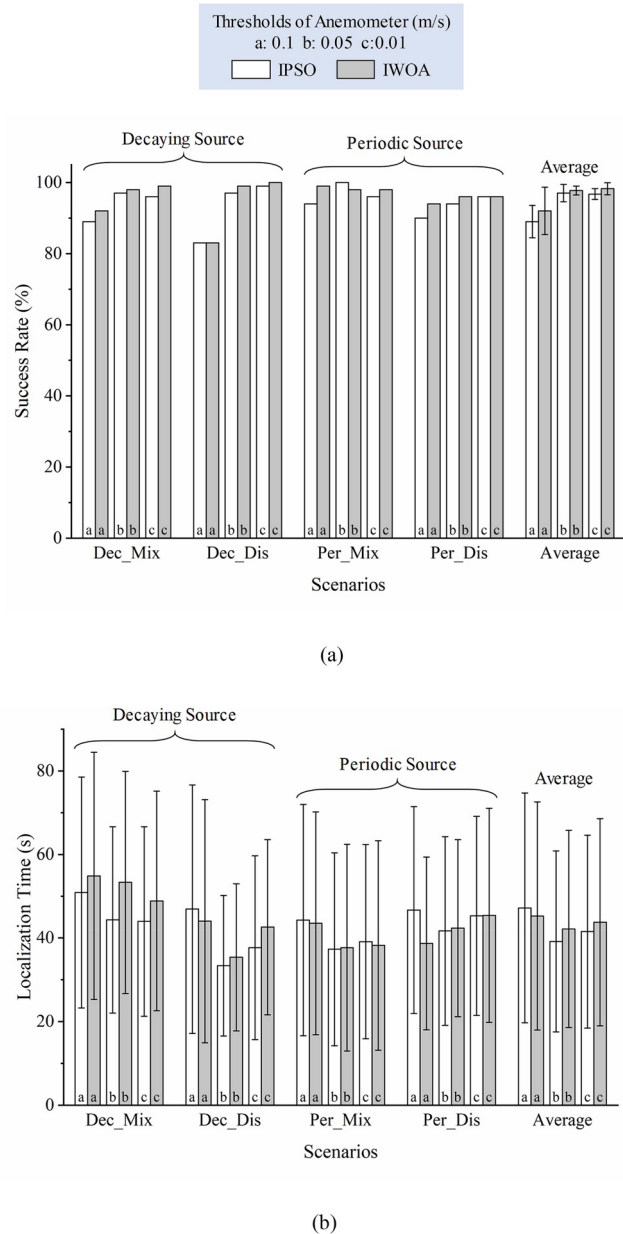


Fig. 19. Source localization results for the IPSO and IWOA methods in four typical scenarios by using anemometers with different measurement thresholds: (a) SR (b) ALT (Dec_Mix: decaying source & mixed ventilation, Dec_Dis: decaying source & displacement ventilation, Per_Mix: periodic source & mixed ventilation, Per_Dis: periodic source & displacement ventilation, Average: averages of the SR and ALT results in four typical scenarios; in each scenario, each method was tested with 100 numerical experiments, and a total of 2400 numerical experiments were conducted).

indoor environments. In the indoor environments where multiple

Appendix A. Statistical tests

To make the statistic results of source localization experiments more credible, another 100 independent experiments were conducted for each scenario using the SWOA and IWOA method with the anemometer's measurement threshold of 0.05 m/s, respectively. The results in Section 4.2 (group A) and those of the additional experiments (group B) are compared in Fig. A1.

particle sources are released simultaneously or sequentially, the source localization problem may be much more difficult. In the future, we will further study how to improve the presented methods to solve the problem of locating multiple indoor particle sources.

5. Conclusion

For locating time-varying indoor particle sources under different ventilation modes, this study presented the SWOA method that uses only concentration information and the IWOA method that uses both concentration and airflow information. These two methods were validated and compared with the SPSO and IPSO methods by combining experiments and CFD simulations, respectively. Four typical scenarios in an experimental chamber, including two time-varying sources (decaying source and periodic source) and two ventilation modes (displacement ventilation and mixing ventilation), were simulated and exported as virtual environments to test these methods. In addition, the effects of the measurement thresholds of anemometers on the performance of the IWOA and IPSO methods were studied to determine the most cost-effective anemometer for source localization. Through this study, the following conclusions can be drawn:

1. The SWOA method generally performed better than the SPSO method in four typical scenarios without using airflow information. Although the SWOA method performed slightly worse than the SPSO method in the decaying source cases, it outperformed significantly in the periodic source cases.
2. The performance of both the SWOA and SPSO methods declined in the periodic source cases. The SR values of the SPSO method (41% and 26%) were too low to meet the requirements of practical applications, while those values of the SWOA method (69% and 56%) were still above an acceptable level. The performance of the SWOA method without using an anemometer shows its application prospects in the development of less expensive and more compact terrestrial robots or micro-UAVs for source localization.
3. Using airflow information can significantly improve the performance of both the IPSO and IWOA methods and achieve high success rates (with a minimum SR value of 89%). The IWOA method performed slightly better in terms of success rate, while the IPSO method performed slightly better in terms of localization efficiency. In addition, this study was able to find the most cost-effective measurement thresholds of anemometers for locating a decaying source (0.05 m/s) and periodic source (0.1 m/s).

Acknowledgments

This study was supported by the National Program on Key Basic Research Project (973 Program) (973 Program, Grant No. 2015CB058003), the National Natural Science Foundation of China (Grant No. 51478468), and the China National Key R&D Program (Grant No. 2018YFC0705201). This study was also supported by the National Natural Science Foundation of China (Grant No. 51708286), and the Natural Science Foundation of Jiangsu Province (Grant No. BK20171015).

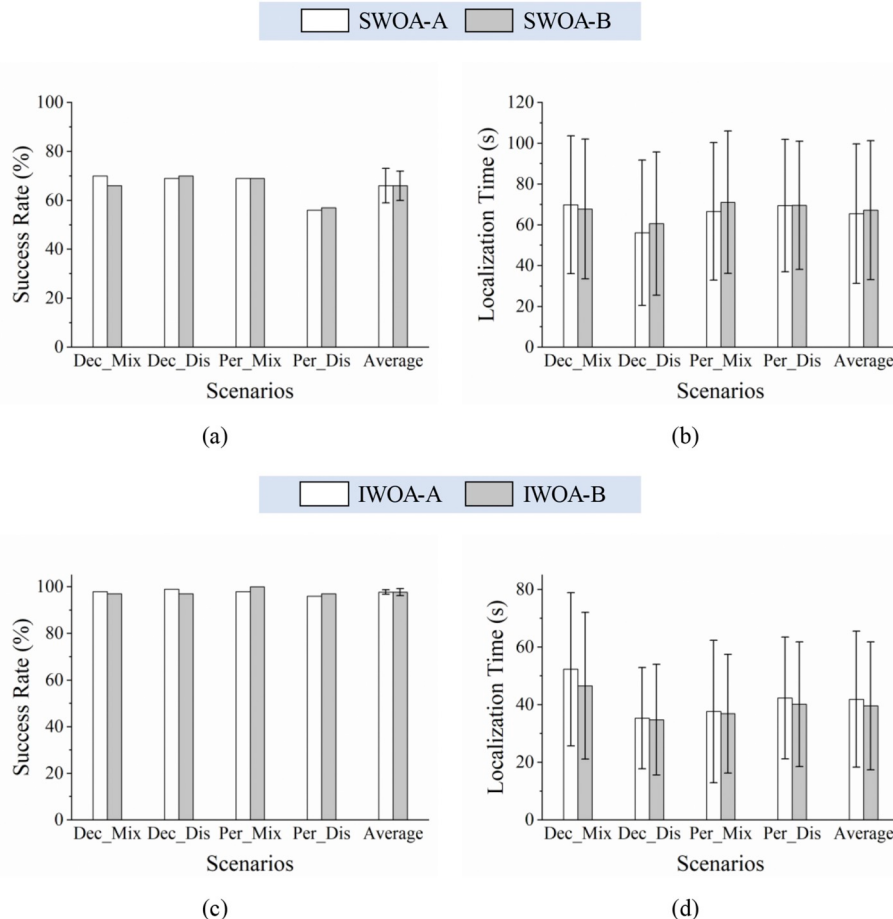


Fig. A1. The source localization results in Section 4.2 (grouped as A) and those of the added experiments (grouped as B): (a) SR of the SWOA method (b) ALT the SWOA method (c) SR of the IWOA method (d) ALT the IWOA method (Dec_Mix: decaying source & mixed ventilation, Dec_Dis: decaying source & displacement ventilation, Per_Mix: periodic source & mixed ventilation, Per_Dis: periodic source & displacement ventilation, Average: averages of the SR and ALT results in four typical scenarios; SWOA-A and IWOA-A: results in Section 4.2; SWOA-B and IWOA-B: results of added experiments for statistical tests).

As shown in Fig. A1, the SRs of groups A and B (SWOA-A and SWOA-B; IWOA-A and IWOA-B) in four scenarios only differed by no more than 2% (Figs. A1 (a) and X(c)). The ALTs and the error bars in Figs. A1 (b) and X(d) are also very close when comparing the results of groups A and B for the same scenario and the same method. These indicates that the results of the two groups were highly consistent in terms of SR.

To further analyze whether the difference between the results in Section 4.2 and those of the additional experiments for each release scenario was significant, the Student's t-test was conducted, and the results were listed in Tables A1 and A2. For each method in each scenario, a null hypothesis was made as follows: $H_0: \mu_A = \mu_B$. As shown in Tables A1 and A2, the t -values were all less than $t_{0.05}(n) \approx 1.984$ ($n \geq 100$), and the p -values were all much higher than 0.05. Therefore, we can accept the null hypothesis that there is no significant difference between the means of groups A and B for each scenario. These results of the Student's t-tests fully proved that 100 independent experiments are sufficient for statistical analysis of the presented methods for each scenario.

Table A1
Results of the Student's t-test for the SWOA method.

Item	Scenarios of source localization			
	Dec_Mix	Dec_Dis	Per_Mix	Per_Dis
A	69.79 ± 33.79	56.10 ± 35.66	66.60 ± 33.73	69.42 ± 32.44
B	67.77 ± 34.22	60.59 ± 35.11	71.07 ± 34.92	69.56 ± 31.40
t	0.420	-0.897	-0.921	-0.031
P	0.675	0.371	0.358	0.975

Table A2

Results of the Student's t-test for the IWOA method.

Item	Scenarios of source localization			
	Dec_Mix	Dec_Dis	Per_Mix	Per_Dis
A	52.32 ± 26.58	35.38 ± 17.58	37.67 ± 24.74	42.35 ± 21.17
B	46.60 ± 25.46	34.82 ± 19.19	36.89 ± 20.64	40.17 ± 21.63
t	1.554	0.215	0.242	0.720
P	0.122	0.830	0.809	0.472

References

- [1] F. Sanchez-Soberon, J. Rovira, J. Sierra, M. Mari, J.L. Domingo, M. Schuhmacher, Seasonal characterization and dosimetry-assisted risk assessment of indoor particulate matter (PM10-2.5, PM2.5-0.25, and PM0.25) collected in different schools, Environ. Res. 175 (2019) 287–296, <https://doi.org/10.1016/j.envres.2019.05.035>.
- [2] A.O. Mocumbi, S. Stewart, S. Patel, W.K. Al-Delaimy, Cardiovascular effects of indoor air pollution from solid fuel: relevance to sub-Saharan Africa, Curr. Environ. Health Rep. 6 (2019) 116–126, <https://doi.org/10.1007/s40572-019-00234-8>.
- [3] L. Pratali, A. Marinoni, A. Cogo, K. Ujka, S. Gilardoni, E. Bernardi, P. Bonasoni, R.M. Bruno, L. Bastiani, E. Vuillermoz, P. Sdringola, S. Fuzzi, Indoor air pollution exposure effects on lung and cardiovascular health in the High Himalayas, Nepal: an observational study, Eur. J. Intern. Med. 61 (2019) 81–87, <https://doi.org/10.1016/j.ejim.2018.10.023>.
- [4] Y. Li, X. Huang, I.T.S. Yu, T.W. Wong, H. Qian, Role of air distribution in SARS transmission during the largest nosocomial outbreak in Hong Kong, Indoor Air 15 (2005) 83–95, <https://doi.org/10.1111/j.1600-0668.2004.00317.x>.
- [5] P. Fabian, J.J. McDevitt, W.H. DeHaan, R.O.P. Fung, B.J. Cowling, K.H. Chan, G.M. Leung, D.K. Milton, Influenza virus in human exhaled breath: an observational study, PLoS One 3 (2008) e2691, <https://doi.org/10.1371/journal.pone.0002691>.
- [6] Z. Liu, S. Ma, G. Cao, C. Meng, B.-J. He, Distribution characteristics, growth, reproduction and transmission modes and control strategies for microbial contamination in HVAC systems: a literature review, Energy Build. 177 (2018) 77–95, <https://doi.org/10.1016/j.enbuild.2018.07.050>.
- [7] D.A. Alexander, S. Klein, Biochemical terrorism: too awful to contemplate, too serious to ignore: subjective literature review, Br. J. Psychiatry J. Ment. Sci. 183 (2003) 491–497.
- [8] W. Blewett, R. Heiden, Protecting buildings and their occupants from airborne hazards, US Army Edgewood Chem. Biol. Cent. ECBC US Army Corps Eng. Pg 1 (2001) 23.
- [9] X. Li, H. Cai, L. Zhao, Antiterrorist Emergency Ventilation: System, Strategy and Decision-Making, Nova Science Publishers, 2009.
- [10] T. Zhang, X. You, Applying neural networks to solve the inverse problem of indoor environment, Indoor Built Environ. 23 (2014) 1187–1195, <https://doi.org/10.1177/1420326X13499596>.
- [11] F. Xue, H. Kikumoto, X. Li, R. Ooka, Bayesian source term estimation of atmospheric releases in urban areas using LES approach, J. Hazard Mater. 349 (2018) 68–78, <https://doi.org/10.1016/j.jhazmat.2018.01.050>.
- [12] T. Zhang, Q. Chen, Identification of contaminant sources in enclosed environments by inverse CFD modeling, Indoor Air 17 (2007) 167–177, <https://doi.org/10.1111/j.1600-0668.2006.00452.x>.
- [13] T. Zhang, Q. Chen, Identification of contaminant sources in enclosed spaces by a single sensor, Indoor Air 0 (2007) 439–449, <https://doi.org/10.1111/j.1600-0668.2007.00489.x>.
- [14] D. Liu, F.-Y. Zhao, H.-Q. Wang, E. Rank, History source identification of airborne pollutant dispersions in a slot ventilated building enclosure, Int. J. Therm. Sci. 64 (2013) 81–92, <https://doi.org/10.1016/j.ijthermalsci.2012.08.005>.
- [15] T. (Tim) Zhang, H. Li, S. Wang, Inversely tracking indoor airborne particles to locate their release sources, Atmos. Environ. 55 (2012) 328–338, <https://doi.org/10.1016/j.atmosenv.2012.03.066>.
- [16] H. Wang, S. Lu, J. Cheng, Z. (John) Zhai, Inverse modeling of indoor instantaneous airborne contaminant source location with adjoint probability-based method under dynamic airflow field, Build. Environ. 117 (2017) 178–190, <https://doi.org/10.1016/j.buildenv.2017.03.017>.
- [17] A.T. Hayes, A. Martinoli, R.M. Goodman, Distributed odor source localization, IEEE Sens. J. 2 (2002) 260–271, <https://doi.org/10.1109/JSEN.2002.800682>.
- [18] X. Chen, J. Huang, Odor source localization algorithms on mobile robots: a review and future outlook, Robot. Auton. Syst. 112 (2019) 123–136, <https://doi.org/10.1016/j.robot.2018.11.014>.
- [19] G. Kowadlo, R.A. Russell, Robot odor localization: a taxonomy and survey, Int. J. Robot. Res. 27 (2008) 869–894, <https://doi.org/10.1177/0278364908095118>.
- [20] A. Bastani, F. Haghhighat, J.A. Kozinski, Contaminant source identification within a building: toward design of immune buildings, Build. Environ. 51 (2012) 320–329, <https://doi.org/10.1016/j.buildenv.2011.12.002>.
- [21] H. Cai, X. Li, Z. Chen, M. Wang, Rapid identification of multiple constantly-released contaminant sources in indoor environments with unknown release time, Build. Environ. 81 (2014) 7–19, <https://doi.org/10.1016/j.buildenv.2014.06.006>.
- [22] Q.-H. Meng, W.-X. Yang, Y. Wang, F. Li, M. Zeng, Adapting an ant colony metaphor for multi-robot chemical plume tracing, Sensors 12 (2012) 4737–4763, <https://doi.org/10.3390/s120404737>.
- [23] Y. Yang, Q. Feng, H. Cai, J. Xu, F. Li, Z. Deng, C. Yan, X. Li, Experimental study on three single-robot active olfaction algorithms for locating contaminant sources in indoor environments with no strong airflow, Build. Environ. 155 (2019) 320–333, <https://doi.org/10.1016/j.buildenv.2019.03.043>.
- [24] Q. Feng, H. Cai, F. Li, X. Liu, S. Liu, J. Xu, An improved particle swarm optimization method for locating time-varying indoor particle sources, Build. Environ. 147 (2019) 146–157, <https://doi.org/10.1016/j.buildenv.2018.10.008>.
- [25] N.P. Gao, J.L. Niu, Modeling particle dispersion and deposition in indoor environments, Atmos. Environ. 41 (2007) 3862–3876, <https://doi.org/10.1016/j.atmosenv.2007.01.016>.
- [26] S. Liu, A. Novoselac, Lagrangian particle modeling in the indoor environment: a comparison of RANS and LES turbulence methods (RP-1512), HVAC R Res. 20 (2014) 480–495, <https://doi.org/10.1080/10789669.2014.884380>.
- [27] V. Tam, R. Higgins, Simple transient release rate models for releases of pressurised liquid petroleum gas from pipelines, J. Hazard Mater. 25 (1990) 193–203, [https://doi.org/10.1016/0304-3894\(90\)85078-H](https://doi.org/10.1016/0304-3894(90)85078-H).
- [28] S. Zhu, S. Kato, S. Murakami, T. Hayashi, Study on inhalation region by means of CFD analysis and experiment, Build. Environ. 40 (2005) 1329–1336, <https://doi.org/10.1016/j.buildenv.2004.11.009>.
- [29] Y. Chen, H. Cai, Z. Chen, Q. Feng, Using multi-robot active olfaction method to locate time-varying contaminant source in indoor environment, Build. Environ. 118 (2017) 101–112, <https://doi.org/10.1016/j.buildenv.2017.03.030>.
- [30] W. Jatmiko, K. Sekiyama, T. Fukuda, A PSO-based mobile robot for odor source localization in dynamic advection-diffusion with obstacles environment: theory, simulation and measurement, IEEE Comput. Intell. Mag. 2 (2007) 37–51, <https://doi.org/10.1109/MCI.2007.353419>.
- [31] Q. Feng, H. Cai, Z. Chen, Y. Yang, J. Lu, F. Li, J. Xu, X. Li, Experimental study on a comprehensive particle swarm optimization method for locating contaminant sources in dynamic indoor environments with mechanical ventilation, Energy Build. 196 (2019) 145–156, <https://doi.org/10.1016/j.enbuild.2019.03.032>.
- [32] Q. Feng, C. Zhang, J. Lu, H. Cai, Z. Chen, Y. Yang, F. Li, X. Li, Source localization in dynamic indoor environments with natural ventilation: an experimental study of a particle swarm optimization-based multi-robot olfaction method, Build. Environ. 161 (2019) 106228, <https://doi.org/10.1016/j.buildenv.2019.106228>.
- [33] L. Marques, U. Nunes, A.T. de Almeida, Particle swarm-based olfactory guided search, Aut. Robots 20 (2006) 277–287, <https://doi.org/10.1007/s10514-006-7567-0>.
- [34] J. Wang, R. Zhang, Y. Yan, X. Dong, J.M. Li, Locating hazardous gas leaks in the atmosphere via modified genetic, MCMC and particle swarm optimization algorithms, Atmos. Environ. 157 (2017) 27–37, <https://doi.org/10.1016/j.atmosenv.2017.03.009>.
- [35] D.-W. Gong, Y. Zhang, C.-L. Qi, Localising odour source using multi-robot and anemotaxis-based particle swarm optimisation, IET Control Theory & Appl. 6 (2012) 1661–1670, <https://doi.org/10.1049/iet-cta.2011.0513>.
- [36] W. Jatmiko, K. Sekiyama, T. Fukuda, A PSO-based mobile sensor network for odor source localization in dynamic environment: theory, simulation and measurement, IEEE Int. Conf. Evol. Comput. (2006) 1036–1043, <https://doi.org/10.1109/CEC.2006.1688423> (2006).
- [37] S. Mirjalili, A. Lewis, The whale optimization algorithm, Adv. Eng. Software 95 (2016) 51–67, <https://doi.org/10.1016/j.advengsoft.2016.01.008>.
- [38] M.A. El Aziz, A.A. Ewees, A.E. Hassanien, Whale optimization algorithm and moth-flame optimization for multilevel thresholding image segmentation, Expert Syst. Appl. 83 (2017) 242–256.
- [39] M. Abdel-Basset, G. Manogaran, D. El-Shahat, S. Mirjalili, A hybrid whale optimization algorithm based on local search strategy for the permutation flow shop scheduling problem, Future Gener. Comput. Syst. 85 (2018) 129–145, <https://doi.org/10.1016/j.future.2018.03.020>.
- [40] D. Prakash, C. Lakshminarayana, Optimal siting of capacitors in radial distribution network using whale optimization algorithm, Alex. Eng. J. 56 (2017) 499–509, <https://doi.org/10.1016/j.aej.2016.10.002>.
- [41] J. Burgués, V. Hernández, A. Lilienthal, S. Marco, Smelling nano aerial vehicle for gas source localization and mapping, Sensors 19 (2019) 478, <https://doi.org/10.3390/s19030478>.
- [42] Q. Chen, Comparison of different k-e models for indoor air flow computations, Numer. Heat Transf. Part B Fundam. 28 (1995) 353–369, <https://doi.org/10.1080/10407799508928838>.
- [43] F. Li, J. Liu, J. Ren, X. Cao, Predicting contaminant dispersion using modified turbulent Schmidt numbers from different vortex structures, Build. Environ. 130 (2018) 120–127, <https://doi.org/10.1016/j.buildenv.2017.12.023>.

- [44] X. Yuan, Y. Wang, J. Liu, X. Xu, X. Yuan, Experimental and numerical study of airflow distribution optimisation in high-density data centre with flexible baffles, *Build. Environ.* 140 (2018) 128–139, <https://doi.org/10.1016/j.buildenv.2018.05.043>.
- [45] Z. Zhang, W. Zhang, Z.J. Zhai, Q.Y. Chen, Evaluation of various turbulence models in predicting airflow and turbulence in enclosed environments by CFD: Part 2—comparison with experimental data from literature, *HVAC R Res.* 13 (2007) 871–886, <https://doi.org/10.1080/10789669.2007.10391460>.
- [46] S. Holmberg, Y. Li, Modelling of the indoor environment–particle dispersion and deposition, *Indoor Air* 8 (1998) 113–122, <https://doi.org/10.1111/j.1600-0668.1998.t01-2-00006.x>.
- [47] W.C. Hinds, *Aerosol Technology: Properties, Behavior, and Measurement of Airborne Particles*, John Wiley & Sons, 1999.
- [48] M.M. Hefny, R. Ooka, CFD analysis of pollutant dispersion around buildings: effect of cell geometry, *Build. Environ.* 44 (2009) 1699–1706, <https://doi.org/10.1016/j.buildenv.2008.11.010>.